Published by Institute of Physics Publishing for SISSA
Received: *March 4, 2005*
Revised: *May 31, 2005*
Accepted: *July 2, 2005*
Published: *August 16, 2005*

New allowed mSUGRA parameter space from variations of the trilinear scalar coupling A_0

Luisa Sabrina Stark,[a] Petra Häfliger,[ab] Adrian Biland[a] and Felicitas Pauss[a]

[a] *Institute for Particle Physics, ETH Zürich*
CH-8093 Zürich, Switzerland
[b] *Paul Scherrer Institute*
CH-5232 Villigen PSI, Switzerland
E-mail: lstark@particle.phys.ethz.ch, petra.haefliger@phys.ethz.ch, biland@particle.phys.ethz.ch, felicitas.pauss@cern.ch

Abstract: In minimal Supergravity (mSUGRA) models the lightest supersymmetric particle (assumed to be the lightest neutralino χ_1^0) provides an excellent cold dark matter (CDM) candidate. The supersymmetric parameter space is significantly reduced, if the limits on the CDM relic density $\Omega_{CDM}h^2$, obtained from WMAP data, are used. Assuming a vanishing trilinear scalar coupling A_0 and fixed values of $\tan\beta$, these limits result in narrow lines of allowed regions in the $m_0 - m_{1/2}$ plane, the so called WMAP strips. In this analysis the trilinear coupling A_0 has been varied within ± 4 TeV. A fixed non vanishing A_0 value leads to a shift of the WMAP strips in the $m_0 - m_{1/2}$ plane.

Keywords: Supergravity Models, Cosmology of Theories beyond the SM.

JHEP08(2005)059

Contents

1. Introduction

The supersymmetric (SUSY[1]) parameter space in minimal Supergravity (mSUGRA) scenarios is usually studied in terms of the common scalar mass m_0, the common gaugino mass $m_{1/2}$, the ratio of the Higgs expectation values $\tan\beta$ and the sign of the Higgsino mass parameter μ. However, the fifth free parameter, the common trilinear scalar coupling A_0, was usually set to zero. In recent studies, the impact of A_0 on the SUSY parameter space was recognised [1].

In the mSUGRA framework the lightest neutralino lends itself as an excellent cold dark matter (CDM) candidate, thus providing a connection between particle physics and astrophysics. The inclusion of cosmological experimental data allows to significantly reduce the mSUGRA parameter space. The satellite born detector WMAP[2] measured the abundance of CDM in the Universe to be $0.094 < \Omega_{CDM}h^2 < 0.129$ (at 2σ C.L.) [2]. Under the assumption of $A_0 = 0\,\mathrm{TeV}$ and fixed $\tan\beta$, only some narrow lines in the $m_0 - m_{1/2}$ plane are left over as allowed regions after including WMAP data [3]. In this analysis we have studied the effects of non vanishing couplings A_0 systematically and found extended areas in the mSUGRA parameter space, which no longer can be excluded. In the next section

[1]In the following the shortcut SUSY is used for supersymmetric as well as Supersymmetry.
[2]`http://map.gsfc.nasa.gov`

we give a short theoretical introduction to SUSY and mSUGRA with particular emphasis on the role of the trilinear scalar coupling A_0. In section 3 we describe the constraints from cosmological data on the mSUGRA parameter space. The tools used for this work are briefly discussed in section 4, including comparisons of the different Monte Carlo (MC) programs. In section 5 we present a scan over the mSUGRA parameter space. Allowing A_0 to vary, the WMAP strips are broadened to extended areas. A general parametrisation of these allowed regions is complicated. Thus, we fixed A_0 to several different values and constructed parametrisations for the resulting lines, which are presented in section 6.

2. Supersymmetry

The Standard Model of particle physics (SM) is in stupendous agreement with experimental measurements. Why should it then be extended? The SM encounters several theoretical problems, which cannot be solved without the introduction of new physics. (i) In the SM the electroweak (EW) symmetry has to be broken in order to generate the masses of the weak gauge bosons. The Higgs sector has been introduced to mediate EW spontaneous symmetry breaking. However, the Higgs mechanism is not experimentally established yet. (ii) The couplings of the three gauge interactions do not unify at some high energy scale, so that the SM cannot easily be included in a grand unified theory (GUT). (iii) Due to quadratically divergent contributions to the Higgs boson mass, the huge gap between the EW and the GUT scale requires the introduction of a fine tuned mass counter term in order to establish an intermediate Higgs mass. This problem is known as the hierarchy problem [4]. (iv) Furthermore, the SM does not provide a candidate for CDM.

SUSY [5, 6] is one of the best motivated candidates for physics beyond the SM. It cannot solve all the problems of the SM but all those listed before. New particles at the TeV scale modify the β-functions of the three gauge couplings such that the latter meet at about 10^{16} GeV [7]. SUSY-GUTs generate the EW symmetry breaking dynamically, if the top mass ranges between about 100 and 200 GeV [8], in agreement with the measured top mass of 172.7 ± 2.9 GeV [9]. By connecting fermions with bosons the hierarchy problem is solved. The quadratic divergences are cancelled systematically order by order, if the corresponding couplings between SM and SUSY particles are identical [4]. Fine tuning of the counter terms is not required, if the masses of the SUSY particles are not too large, i.e. of the $\mathcal{O}$(TeV). The lightest supersymmetric particle (LSP), if stable, provides a good candidate for CDM [10]. However, several problems of the SM remain unexplained in SUSY extensions of the SM as e.g. the masses of the fermions or the origin of three generations.

2.1 MSSM

The minimal supersymmetric extension of the SM (MSSM) [6], requires a doubling of the SM degrees of freedom (d.o.f.) including two complex Higgs doublets $H_d = (H_d^0, H_d^-)$ and $H_u = (H_u^+, H_u^0)$ giving mass to the down-type and up-type fermions, respectively. For each fermionic d.o.f. a corresponding bosonic one exists and vice versa, as can be inferred from table 1. Two complex Higgs doublets are needed for the theory to be supersymmetric and free of anomalies. After spontaneous symmetry breaking five of the eight states remain

JHEP08(2005)059

Gauge Multiplets		Chiral Multiplets	
$J = 1$	$J = 1/2$	$J = 1/2$	$J = 0$
Gluon g	Gluino $\tilde{g}$	Quark Q	Squark $\tilde{Q}_{1,2}$
$W^{\pm}$, W^0	Wino $\tilde{W}^{\pm}$, $\tilde{W}^0$	Lepton L	Slepton $\tilde{L}_{1,2}$
B^0	Bino $\tilde{B}^0$	Higgsino $\tilde{H}_d^0$, $\tilde{H}_d^-$, $\tilde{H}_u^+$, $\tilde{H}_u^0$	Higgs H_d, H_u

Table 1: Particle content of the MSSM. The gauge multiplets mediate the interactions while the chiral multiplets contain the matter content. J denotes the spin quantum number.

as physical particles: two neutral CP-even (scalar), one neutral CP-odd (pseudoscalar) and two charged Higgs bosons. The scalar superpartners of the left/right-handed fermion components $\tilde{Q}_L, \tilde{u}_R, \tilde{d}_R$ and $\tilde{L}_L, \tilde{e}_R$ mix with each other yielding the mass eigenstates $\tilde{Q}_{1,2}$ and $\tilde{L}_{1,2}$, respectively [6]. Since the mixing angles are proportional to the masses of the ordinary fermions, mixing effects are only important for the third-generation sfermions. The four neutralinos $\chi^0_{1...4}$ are linear combinations of the SUSY partners of the neutral gauge bosons $\tilde{W}^0$, $\tilde{B}^0$ and the neutral Higgsinos $\tilde{H}^0_{u,d}$, the superpartners of the neutral components of the two Higgs doublets. Analogously the charged winos $\tilde{W}^{\pm}$ and the charged Higgsinos $\tilde{H}_u^+$, $\tilde{H}_d^-$ build up the four charginos $\chi^{\pm}_{1,2}$ as mass eigenstates.

The R-parity [11], defined as $R = (-1)^{3B+2S+L}$ with B = baryon number, S = spin and L = lepton number is introduced as a new discrete symmetry, which distinguishes SM particles ($R = 1$) and their SUSY partners ($R = -1$). In R-parity conserving models the SUSY particles (sparticles) can only be produced/annihilated in pairs, so that the LSP is stable.

2.2 mSUGRA

Since no SUSY particle with the same mass as its SM partner has been discovered, SUSY has to be broken. Different scenarios for SUSY breaking mechanisms have been proposed. It is typically assumed, that the breaking takes place at a high energy scale. There are several models with different messenger particles (gravitons, gauge bosons, ...) mediating the SUSY breaking effects down to the EW scale. We concentrate on mSUGRA models with the graviton as the messenger particle [12]. The key point of these models is the unification of the bosonic masses to the common scalar mass m_0, of the fermionic masses to the common gaugino mass $m_{1/2}$ and of the trilinear scalar couplings to A_0 at the GUT scale in addition to gauge coupling unification. As a consequence, the whole MSSM can be described by only five additional parameters to the SM ones (instead of more than 100 parameters as in the general MSSM): m_0, $m_{1/2}$, A_0, $\tan\beta$ and $\mathrm{sign}(\mu)$, the sign of the Higgsino mass parameter. All parameters of the MSSM can be derived by renormalisation group (RG) equations from the values of these five input parameters (which define a specific mSUGRA model) at the GUT scale, as illustrated in figure 1.

In R-parity conserving mSUGRA models the LSP is a neutralino in large regions of the parameter space, if cosmological bounds are taken into account [2]. As the χ^0_1 is electrically

JHEP08(2005)059

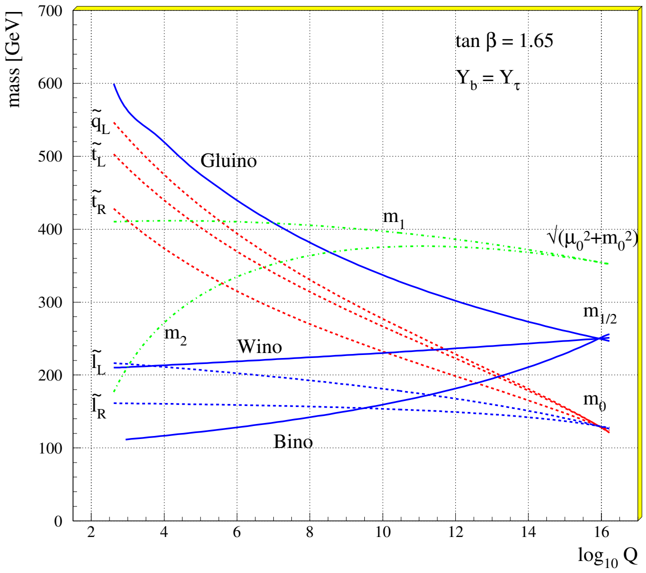

Figure 1: Unification of the sparticle masses at the GUT scale [13]. The common gaugino mass $m_{1/2}$ and the common scalar mass m_0 are input parameters of mSUGRA.

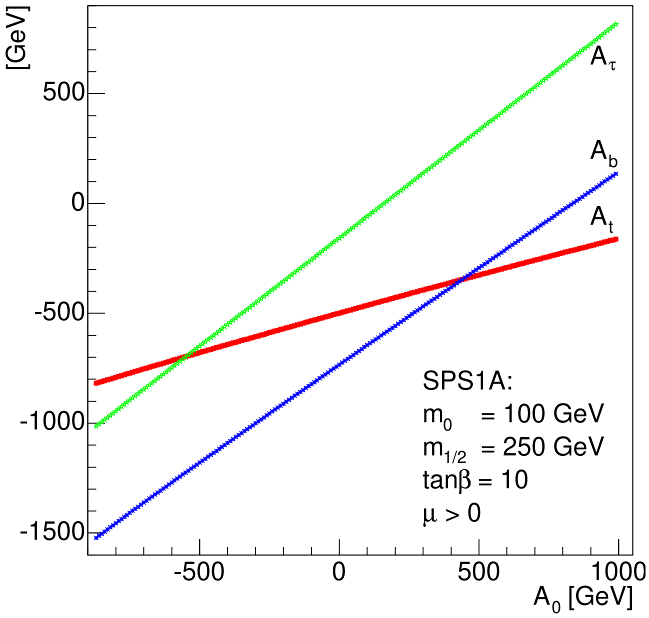

Figure 2: Dependence of the trilinear scalar couplings A_t, A_b and A_τ at the EW scale on A_0 for the Snowmass point SPS1A [14]. Values of A_0 outside the displayed region are excluded because of numerical problems of the RG equations.

neutral, it does not directly couple to photons, an essential condition for any dark matter candidate.

2.3 Trilinear scalar coupling A_0

In figure 2 the linear A_0 dependence of the trilinear couplings of the third generation, $A_{t,b,\tau}$,

JHEP08(2005)059

is depicted. The evolution of A_0 down to the EW scale determines the couplings $A_{u,d,l}$ for up/down-type squarks and charged sleptons resulting in the approximate relation:

$$A_k = d_k A_0 + d'_k m_{1/2}$$

with $k = u, d, l$. The coefficients d_k depend on the corresponding Yukawa couplings and are of $\mathcal{O}(1)$, increasing for decreasing masses. As the top quark is much heavier than the bottom quark and the tau lepton, the slope of A_t is smaller for small $\tan\beta$ (figure 2). The coefficients d'_k depend additionally on the gauge couplings and are of order unity [15]. The RG evolution of $A_{u,d,l}$ from the GUT to the EW scale generates the corresponding terms of the SUSY breaking part of the lagrangian in the low energy limit:

$$\mathcal{L}_{\text{soft}} = \frac{g}{\sqrt{2}M_W}\varepsilon_{ij}\left[\frac{M_u}{\sin\beta}A_u H_u^i \tilde{Q}_L^j \tilde{u}_R^\dagger + \frac{M_d}{\cos\beta}A_d H_d^i \tilde{Q}_L^j \tilde{d}_R^\dagger + \frac{M_l}{\cos\beta}A_l H_d^i \tilde{L}_L^j \tilde{e}_R^\dagger\right], \quad (2.1)$$

where g denotes the coupling constant of $\mathrm{SU}(2)_L$ and ε_{ij} is the two-dimensional anti-symmetric tensor. M_W is the mass of the W boson and $M_{u,d,l}$ are the masses of the up/down-type quarks and the charged leptons, respectively. These terms of the lagrangian introduce interactions between MSSM Higgs bosons, "left-" and "right-handed" sfermions, in addition to the usual interaction mediated by the Yukawa couplings. These additional couplings are proportional to the masses of the corresponding fermions (eq. (2.1)), so that they are only relevant for the third generation.

3. Relic density

In the early Universe the interaction rate (Γ) of a species of particles must be larger than the expansion rate of the Universe. Otherwise the thermal equilibrium cannot be maintained and the particles decouple at the freeze out temperature T_f, i.e. if the following condition is fulfilled:

$$\Gamma = n\langle\sigma v\rangle = H \qquad \text{at} \quad T_f\,, \quad (3.1)$$

where n denotes the number density of the particle species, H is the Hubble constant and $\langle\sigma v\rangle$ is the thermal average of the total annihilation cross section times the velocity of the corresponding particles. The ratio of the number of relic particles to the total entropy in the Universe remains constant after they are frozen out. Since the present entropy density is known, the present number of these particles can be approximately determined by using the freeze out condition (eq. (3.1)). The relic density of a particle species X can be estimated as [16]:

$$\Omega_X h^2 \approx \frac{3\times 10^{-27}\ cm^3 s^{-1}}{\langle\sigma v\rangle_X}\,,$$

where h denotes the Hubble constant in units of 100 km sec^{-1} Mpc^{-1}. The cross section is proportional to the squared matrix element. The matrix element for a given process is inversely proportional to the squared mass of a heavy propagator particle. Assuming SUSY CDM, the propagator particle may also be a sparticle. In the case of neutralino annihilation, the cross section contains several different channels, thus the dependence of $\Omega_\chi h^2$ on the mSUGRA parameters is not trivial.

JHEP08(2005)059

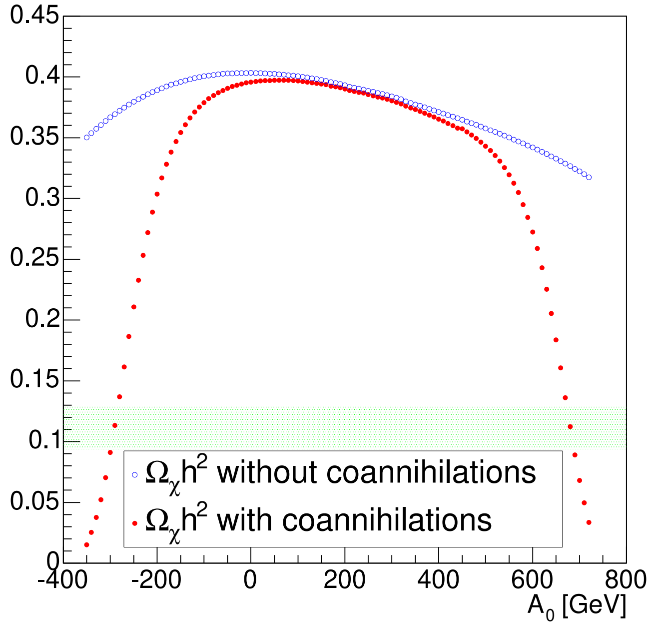

Figure 3: Difference between the values of the relic density for calculations without (blue circles) and with (red points) coannihilation processes. The input parameters are taken from the Snowmass point SPS1B ($m_0 = 200\,\mathrm{GeV}$, $m_{1/2} = 400\,\mathrm{GeV}$, $\tan\beta = 30$, $\mu > 0$) and A_0 has been varied within ± 1 TeV. The green shaded area shows the region allowed by the WMAP data.

Moreover, it is important to include all possible coannihilation processes [17] between the LSP and the next heavier sparticles as can be inferred from figure 3 for the Snowmass benchmark point SPS1B ($m_0 = 200\,\mathrm{GeV}$, $m_{1/2} = 400\,\mathrm{GeV}$, $\tan\beta = 30$, $\mu > 0$) [14]. A_0 has been varied within $\pm 1\,\mathrm{TeV}$.[3] Without coannihilations the Snowmass point SPS1B would be excluded by the WMAP data. Including coannihilations several models with $A_0 \neq 0\,\mathrm{TeV}$ are allowed. The formulas including coannihilations are more involved [17].

The relic neutralino density (incl. coannihilation) for $\tan\beta = 10$, $A_0 = -500\,\mathrm{GeV}$ and $+2000\,\mathrm{GeV}$ as a function of $m_{1/2}$ with $0 < m_0 < 300\,\mathrm{GeV}$ is depicted in figure 4. The lines result from fixed values of m_0, the step sizes for $m_0, m_{1/2}$ are chosen to be 5 GeV for both plots. This is exemplified by the red lines, which correspond to $m_0 = 190\,\mathrm{GeV}$ in the left plot and to $m_0 = 235\,\mathrm{GeV}$ in the right plot in figure 4. Values below the red lines belong to smaller m_0 values and lines above to larger ones. Models with $m_{1/2} \lesssim 170\,\mathrm{GeV}$ in the left plot and with $m_{1/2} \lesssim 480\,\mathrm{GeV}$ in the right plot are excluded by collider constraints. With growing $m_{1/2}$ the lower limit of the relic density becomes larger.

Assuming that CDM entirely consists of LSPs, the application of cosmological constraints on the mSUGRA parameter space is possible. The WMAP experiment constrained the relic CDM density to the narrow range $0.094 < \Omega_{CDM}h^2 < 0.129$. For vanishing A_0, only some narrow strips remain as can be inferred from figure 5. The left plot has been obtained by the authors of ref. [3] using their own Monte Carlo programs. The parametrisation of these data defines the WMAP strips (black lines in the right plot). The right plot

[3] Numerical problems of the RGEs occur for $A_0 < -350\,\mathrm{GeV}$ and $A_0 > 720\,\mathrm{GeV}$.

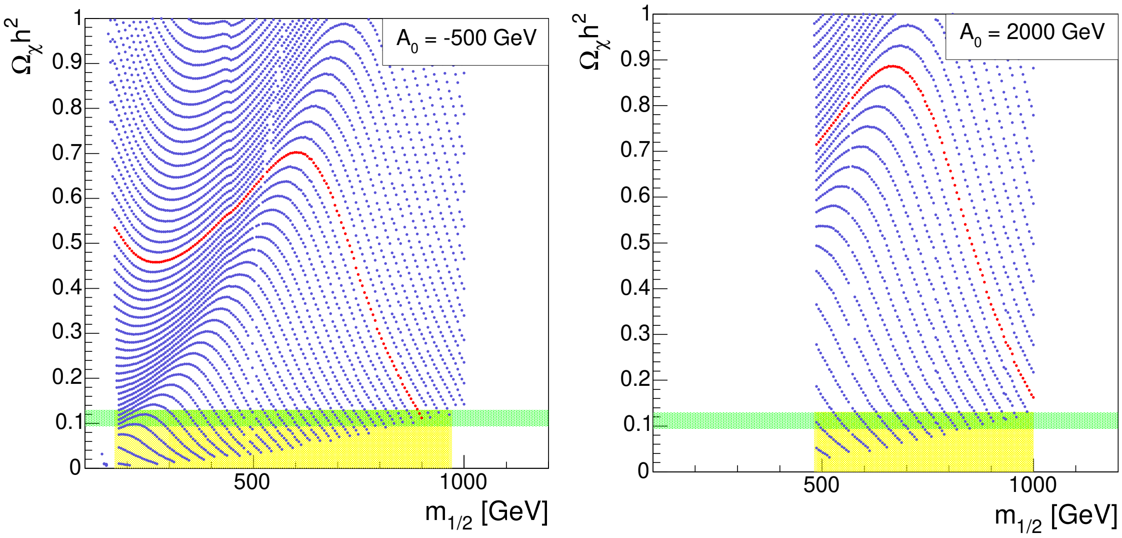

Figure 4: The relic density $\Omega_\chi h^2$ as a function of $m_{1/2}$ obtained using the ISAJET and the DarkSUSY Monte Carlo programs, for $\tan\beta = 10$, $\mu > 0$, $m_{1/2} \leq 1\,\mathrm{TeV}$, m_0 varied between 0 and 300 GeV and $A_0 = -500\,\mathrm{GeV}$ (left) and $A_0 = 2000\,\mathrm{GeV}$ (right). The red lines belong to $m_0 = 190\,\mathrm{GeV}$ (left) and $m_0 = 235\,\mathrm{GeV}$ (right). Each single point denotes one set of mSUGRA parameters. The green shaded area shows the region allowed by the WMAP data and the yellow shaded area indicates the resulting allowed $m_{1/2}$ region.

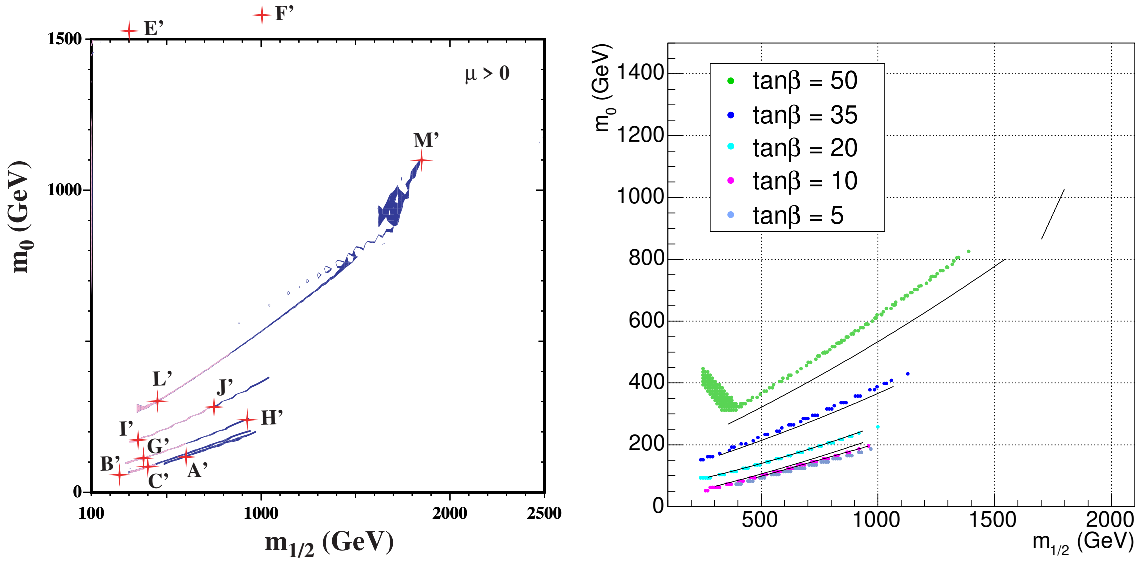

Figure 5: Regions in the $m_0 - m_{1/2}$ plane accounting for $0.094 < \Omega_\chi h^2 < 0.129$ for different $\tan\beta$, $\mu > 0$ and $A_0 = 0\,\mathrm{TeV}$. Left plot: WMAP strips (for $m_t = 175\,\mathrm{GeV}$) from ref. [3] are shown with the post WMAP benchmark points (A'…M'). Right plot: The corresponding allowed regions obtained with ISAJET and DarkSUSY are shown for $m_t = 178\,\mathrm{GeV}$. The black lines are the parametrisation given for the WMAP strips in the left plot.

displays the results of this study, using the ISAJET and DarkSUSY Monte Carlo generators, for comparison. For small values of $\tan\beta$ the agreement is good, but the differences increase with $\tan\beta$. The mSUGRA models with large values of $\tan\beta, m_0$ and $m_{1/2}$, shown in the left plot (in vicinity of M'), are excluded in the right plot since the relic densities are too large. The extended region for $\tan\beta = 50$ and small values of m_0, $m_{1/2}$ obtained with ISAJET does not show up in the left plot. If we include variation of the parameter A_0 within ± 4 TeV, the WMAP strips are broadened to extended areas as will be shown in section 5.

4. Monte Carlo generators

As already stated in section 2, the RG equations have to be applied to evolve the mSUGRA parameters from the GUT scale down to the EW scale. For these evolutions two different Monte Carlo programs have been used:

1. **SuSpect** [18]: SuSpect 2.2 is a Fortran code used to determine the SUSY particle spectra. The calculations are done in the MSSM framework assuming R-parity and CP conservation. It can also be applied to constrained scenarios as mSUGRA, anomaly mediated SUSY breaking (AMSB) and gauge mediated SUSY breaking (GMSB) models. The algorithm incorporates RG equations to evolve the parameters between the EW and the GUT scale complemented by constraints from radiative EW symmetry breaking.
2. **ISAJET** [19]: the ISAJET 7.69 package contains ISASUSY, which treats the production and decays of supersymmetric particles. The calculations are done within the MSSM framework, if the input parameters are provided at the EW scale. The ISAJET package provides in addition the possibility to choose the input parameters at the GUT scale and then to perform the RG evolution down to the EW scale.

The generated SUSY spectra have been linked [20] to the **DarkSUSY** program to calculate the relic density.

3. **DarkSUSY** [21]: DarkSUSY 4.00 is currently one of the most advanced programs to perform DM calculations in a SUSY framework. It computes the relic density of the lightest neutralino which is assumed to be the DM particle. The calculations include the impacts of resonances, pair production thresholds and coannihilation processes [17]. To check the validity of the input parameters the presently known bounds from accelerators are included. This package also computes fluxes for a large variety of detector types.

4.1 Differences between SuSpect and ISAJET

As the implementation of the RG evolution is different in the two programs, small differences in the SUSY spectra and couplings arise as shown in figures 6 and 7.[4] The mass spectra provided by these two programs agree at a level of about 10% for models with m_0 not much larger than $m_{1/2}$ and not too large values of $\tan\beta$. However, the calculated

[4]Models with A_0 larger or smaller than displayed are excluded because of problems in the numerical application of the RG equations.

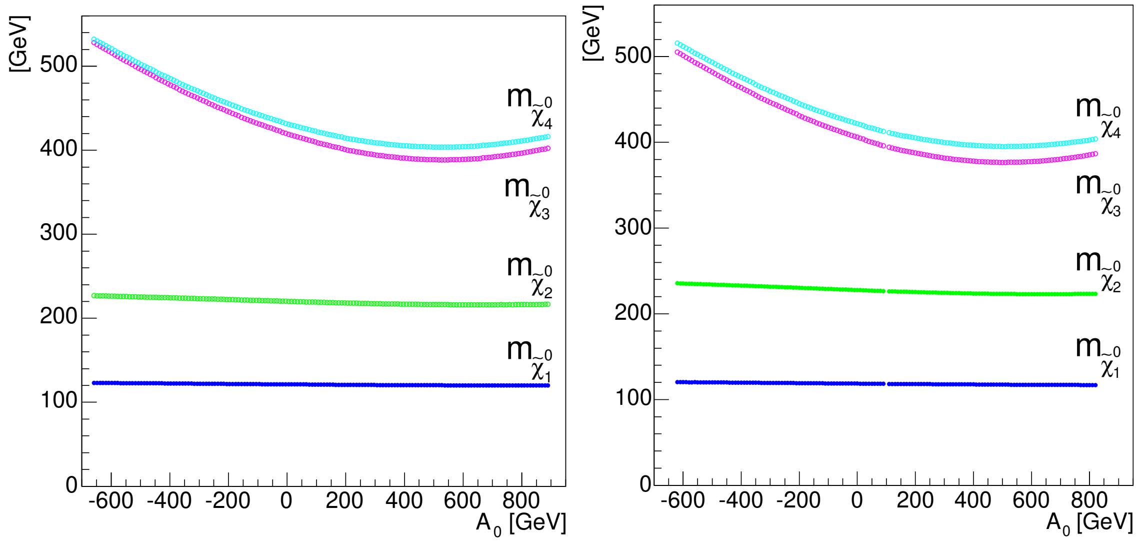

Figure 6: Neutralino masses as a function of A_0 obtained with the SuSpect (left) and the ISAJET (right) programs for the Snowmass point SPS4 ($m_0 = 400\,\mathrm{GeV}$, $m_{1/2} = 300\,\mathrm{GeV}$, $\tan\beta = 50$, $\mu > 0$).

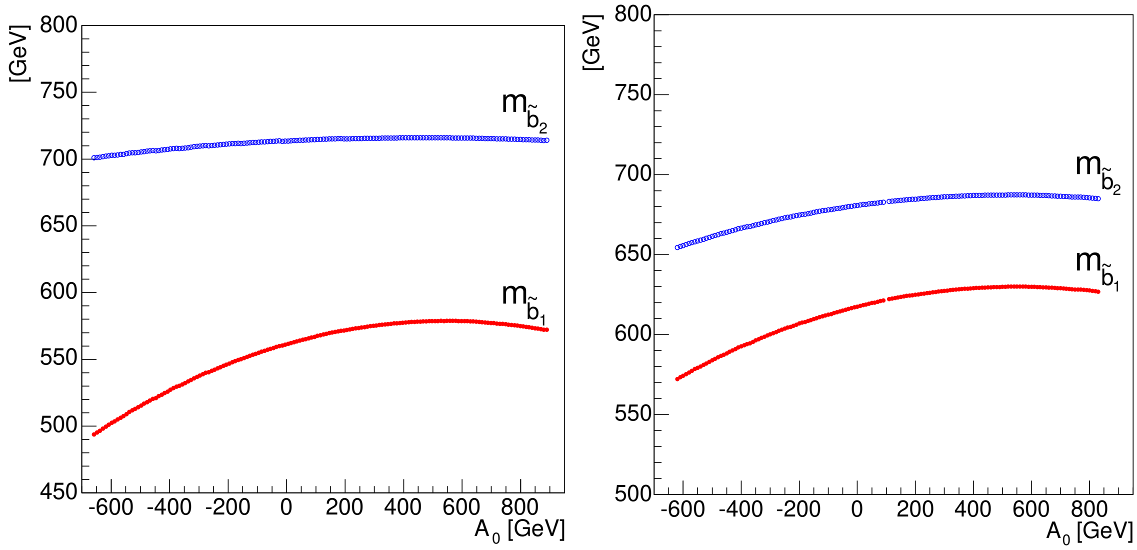

Figure 7: Masses of the two sbottom squarks for the Snowmass point SPS4. The masses in the left/right plot are computed with SuSpect/ISAJET.

SUSY masses can differ by more than a factor of 2 for models in the focus point region or large tanβ values [22]. The neutralino masses calculated by the two programs agree quite well, e.g. for the Snowmass point SPS4 ($m_0 = 400\,\mathrm{GeV}$, $m_{1/2} = 300\,\mathrm{GeV}$, $\tan\beta = 50$, $\mu > 0$): in figure 6 the masses of the four neutralinos are shown as a function of A_0. The LSP mass is independent of A_0 and the approximate mass degeneration as well as the A_0 dependence of the two heavy neutralinos is clearly visible.

However, for the same SPS benchmark point the masses of the sbottom squarks agree only on the 10% level between the two programs, as indicated in figure 7. This difference

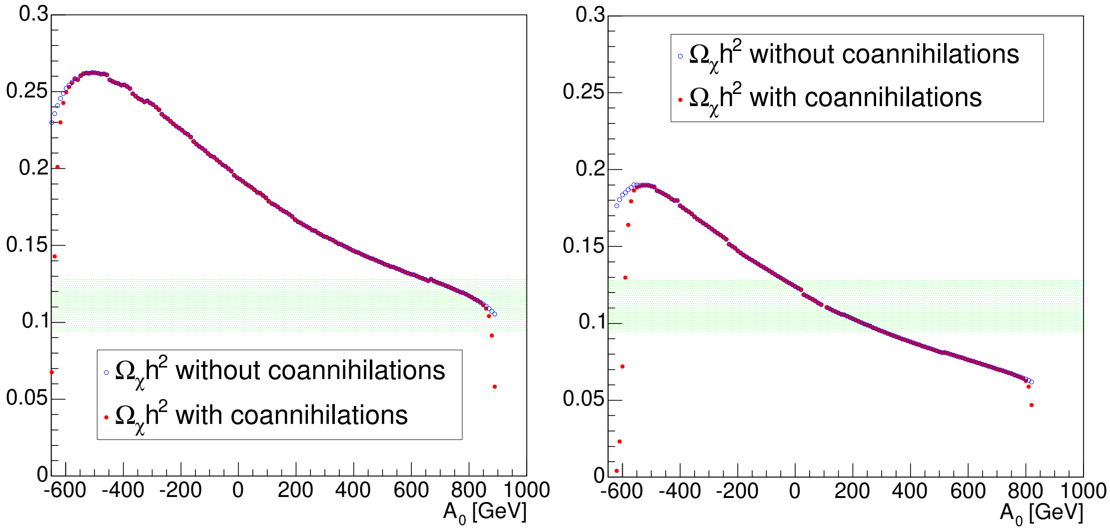

Figure 8: Relic density as a function of A_0, obtained with the SuSpect (left) and ISAJET (right) programs for the Snowmass point SPS4. The blue circles correspond to a calculation without any coannihilation processes, while the red points include coannihilations. The green shaded region marks the allowed regions by the WMAP data.

directly affects the relic density calculations because of significant sbottom exchange contributions in the neutralino annihilation process. Due to the smaller sbottom mass $m_{\tilde{b}_1}$ calculated by SuSpect, the resulting relic density (figure 8) is larger than the corresponding ISAJET value. Since the WMAP constraints on the relic density are quite strong, the number of models, which survive these constraints are different for SuSpect and ISAJET as demonstrated in figure 9. Moreover, the regions in $m_{1/2}$, allowed by the WMAP data for fixed values of A_0, are different, too.

5. Scan of the supersymmetric parameter space

Assuming CDM to consist exclusively of neutralinos, the cosmological bounds on the neutralino relic density $\Omega_\chi h^2$ imply strong constraints on the mSUGRA parameter space. Since the aim of this analysis is to investigate the impact of A_0 on the allowed regions in the mSUGRA parameter space, we varied A_0 in a first step, while keeping the other four parameters fixed. For this study we have chosen the Snowmass points [14] as benchmarks. In a second step we also varied m_0 and $m_{1/2}$ for different but fixed values of $\tan\beta$. Recent data for $(g-2)_\mu$ favour a positive value of the Higgsino mass parameter [23], therefore we focused our analysis on $\mu > 0$. A few million mSUGRA models have been generated for the remaining four input parameters. We varied m_0 and $m_{1/2}$ between 0 and 2 TeV, $\tan\beta$ between 5 and 50 and A_0 within ± 4 TeV. For the calculations the mass of the top quark has been set to 178 GeV.

For all these models the relic density Ω_χ has been computed and required to be within $0.094 < \Omega_\chi h^2 < 0.129$. In addition, the accelerator constraints adopted from the 2002 limits of the Particle Data Group have been taken into account [24]. There are some updates of these constraints [25], including the rare decay $b \to s\gamma$. The accelerator constraints are applied to the mass spectra at the EW scale.

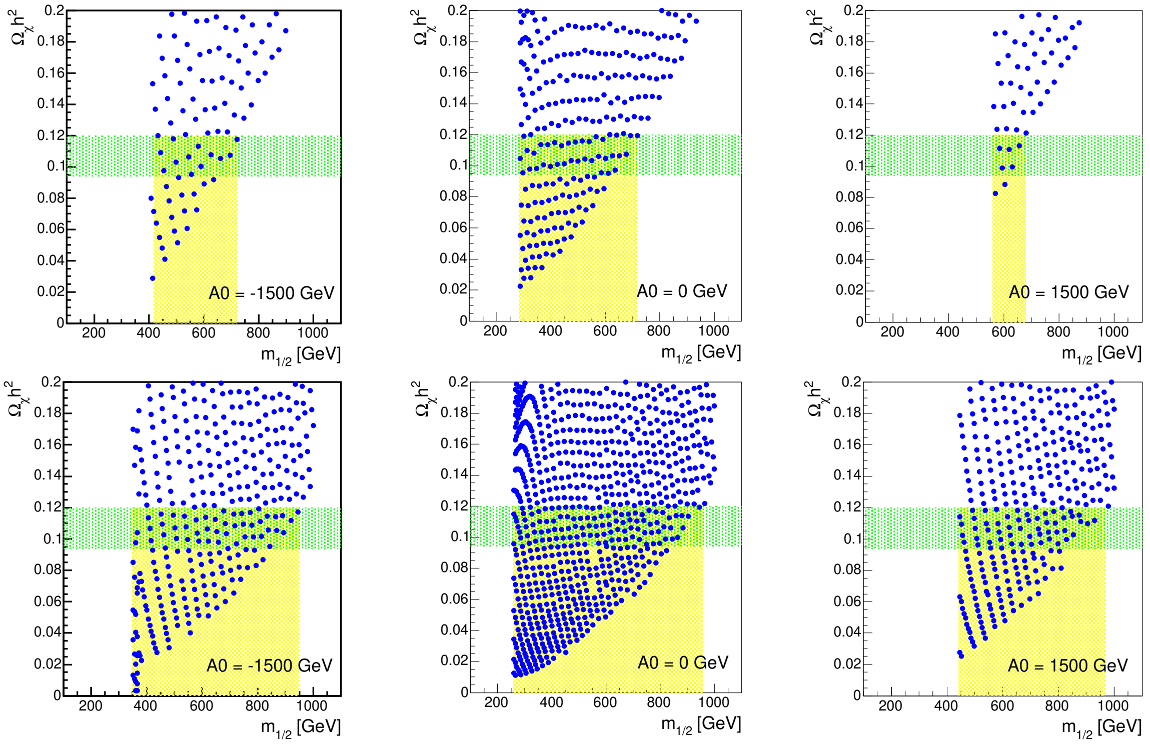

Figure 9: Relic density as a function of $m_{1/2}$ obtained with the SuSpect (top row) and ISAJET (bottom row) programs for $\tan\beta = 10$, $\mu > 0$ and different values of A_0. The green shaded regions mark the WMAP allowed region. The yellow shaded regions show the corresponding $m_{1/2}$ ranges, which can differ significantly for the two MC programs.

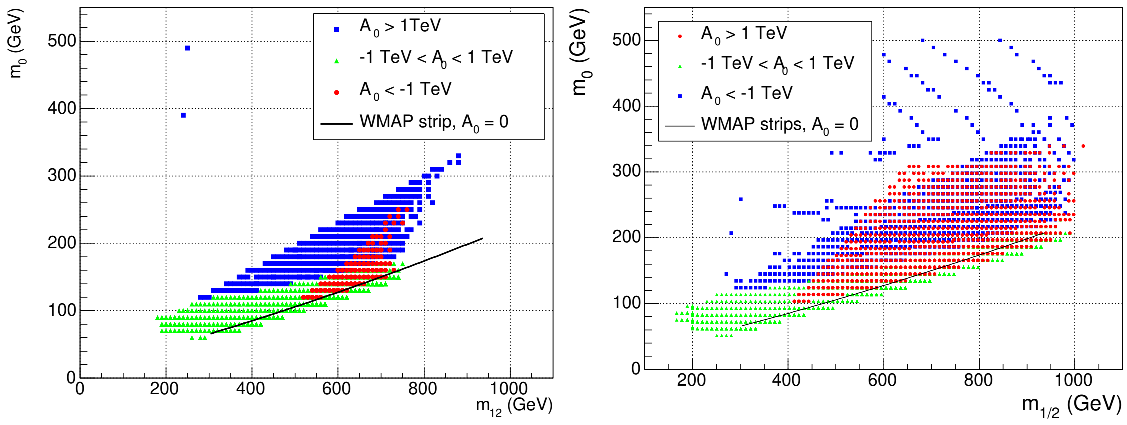

Figure 10: Allowed models in the $m_0 - m_{1/2}$ plane for $\tan\beta = 10$ and $\mu > 0$ obtained with SuSpect (left) / ISAJET (right). The black line corresponds to the WMAP strip for $A_0 = 0\,\text{TeV}$ from ref. [3].

Figure 10 shows that the WMAP strip described in [3] broadens significantly, if A_0 is allowed to vary. The extension of the allowed regions originates mainly from larger values of m_0, which are allowed for non-vanishing A_0, while the minimal m_0 values are obtained for $A_0 = 0\,\text{TeV}$. Large values of $m_{1/2}$ are excluded by the WMAP constraints on the relic density. Since slightly larger values of $\Omega_\chi h^2$ are derived by SuSpect than by ISAJET, more

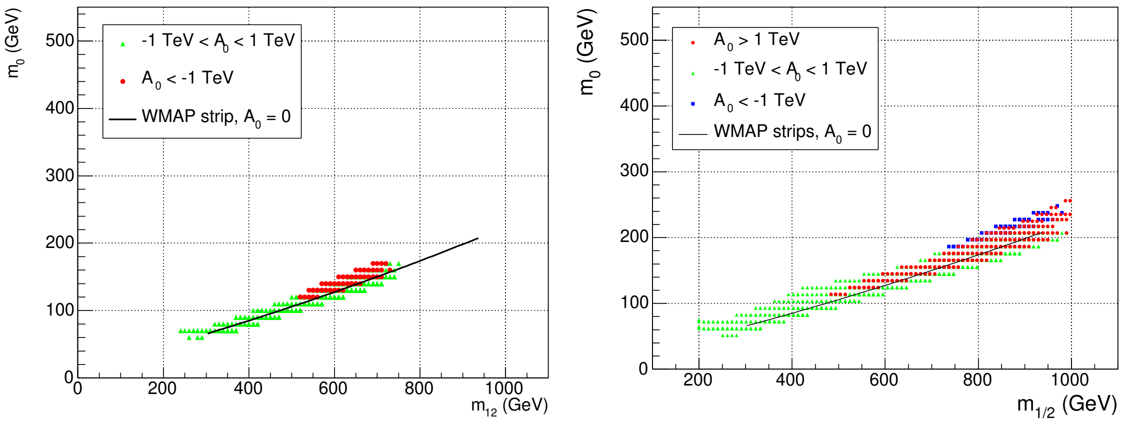

Figure 11: Allowed models in the $m_0 - m_{1/2}$ plane for $\tan\beta = 10$ and $\mu > 0$ obtained with SuSpect (left) / ISAJET (right) after applying the cuts on $A_{t,b,\tau}$ to avoid colour and/or charge breaking. The black line corresponds to the WMAP strip for $A_0 = 0\,\text{TeV}$ from ref. [3].

SuSpect models with larger $m_{1/2}$ are excluded. The parametrisation of the WMAP strips (black lines in figure 10) have been determined with other programs [3], thus introducing small differences with respect to our analysis. In order to avoid colour and/or charge breaking the trilinear scalar couplings at the EW scale $A_{t,b,\tau}$ have to be approximately constrained as [26]:

$$\begin{aligned} A_t^2 &\le 3(m_{H_u}^2 + m_{\tilde{Q}_L}^2 + m_{\tilde{t}_R}^2) \\ A_b^2 &\le 3(m_{H_d}^2 + m_{\tilde{Q}_L}^2 + m_{\tilde{b}_R}^2) \\ A_\tau^2 &\le 3(m_{H_d}^2 + m_{\tilde{L}_L}^2 + m_{\tilde{\tau}_R}^2)\,. \end{aligned} \tag{5.1}$$

The consequences of applying these cuts is depicted in figure 11 for $\tan\beta = 10$ and $\mu > 0$. About 35% of the mSUGRA models, generated with SuSpect, satisfying the WMAP constraints are excluded, while for ISAJET the impact of these cuts is even stronger, i.e. about 45% of the models are rejected (figure 11). By far the biggest effect originates from the cut on A_τ due to the light stau masses $m_{\tilde{\tau}_{L,R}}$. Most of the models (more than 90%) with $A_0 < -1\,\text{TeV}$ are excluded by the cut. Models with A_0 values larger than $1\,\text{TeV}$ are significantly affected, too (about 40%).

To avoid CCB these cuts are necessary but not sufficient, since the vacuum expectation values of the squarks, the sleptons and the corresponding Higgs boson were assumed to be equal, for simplicity. Moreover, these bounds (eq. (5.1)) were derived from the tree level scalar potential, while radiative corrections are expected to modify them.

The scalar potential may contain global CCB minima in addition to the local EW breaking minima. As no CCB has been observed, the Universe in its present state may be trapped in a local EW breaking minimum. Since this metastable state may have a lifetime longer than the age of the Universe due to the small tunnelling probability into the global minimum [27], CCB cannot be excluded. Thus, we did not apply these cuts in this analysis.

In figure 12 all allowed models for different values of the trilinear scalar coupling A_0 and $\tan\beta$ are shown in the $m_0 - m_{1/2}$ plane assuming the Higgsino mass parameter μ

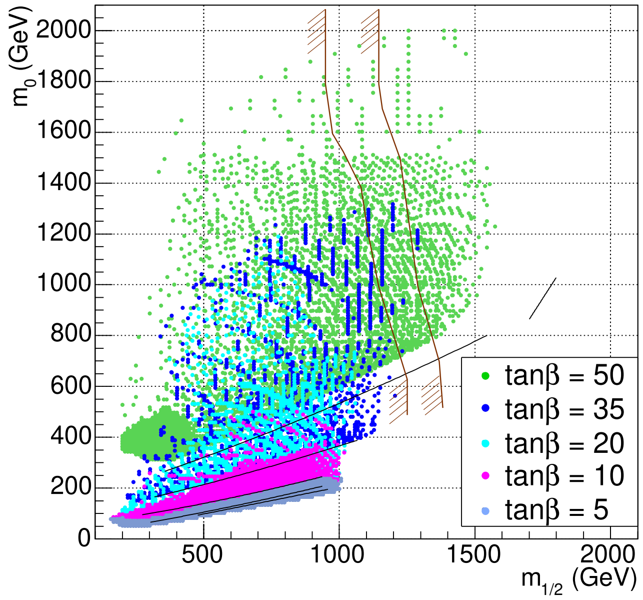

Figure 12: Allowed models in the $m_0 - m_{1/2}$ plane for $m_0, m_{1/2} \le 2\,\mathrm{TeV}$, $\tan\beta$ between 5 and 50, $\mu > 0$ and A_0 within $\pm 4\,\mathrm{TeV}$ from ISAJET. The black lines correspond to the WMAP strips as parametrised in ref. [3], with $\tan\beta = 5$, 10, 20, 35 and 50, where $\tan\beta = 5$ belongs to the lowest black line and $\tan\beta = 50$ to the highest one. The brown lines indicate the LHC discovery reach for an integrated luminosity of $100\,\mathrm{fb}^{-1}$ and $300\,\mathrm{fb}^{-1}$ [28], respectively.

to be positive. This plot corresponds to figure 10 but with $\tan\beta = 5$, 10, 20, 35 and 50 superimposed. In contrast to figure 5, where only a few lines survived the WMAP constraints, extended regions in the mSUGRA parameter space are allowed, if A_0 is not fixed. For $\tan\beta = 10$ mSUGRA models with $m_0 \sim 350\,\mathrm{GeV}$ for largely negative A_0 are within the WMAP constraints, while for $A_0 = 0\,\mathrm{TeV}$ the upper bound was about $m_0 \sim 200\,\mathrm{GeV}$. The analogous behaviour can be observed for larger $\tan\beta$ values, where mSUGRA models with m_0 around $2\,\mathrm{TeV}$ are allowed for large $|A_0|$.

The masses of the gluinos, of the first two squark generations and of the light scalar Higgs boson are nearly independent of A_0. Since the squarks of the first two generations are almost degenerated in mass, only $m_{\tilde{u}_1}$ is shown in figure 13 as a representative example. However, the third generation squark masses $m_{\tilde{b}_{1,2}}$, $m_{\tilde{t}_{1,2}}$ as well as the heavier Higgs masses $m_{H,A,H^\pm}$ depend on the trilinear coupling A_0 in general. The future Large Hadron Collider (LHC), with an anticipated luminosity of $100\,\mathrm{fb}^{-1}$, will cover the $m_{1/2}$ domain up to about $\mathcal{O}(\mathrm{TeV})$, almost independent of m_0 [28] (brown contours in figure 12). Thus, most of the models generated in this analysis are within the reach of the LHC.

6. Parametrisation

As can be inferred from figures 14, 15 and 16 the allowed regions in the $m_0 - m_{1/2}$ plane correspond to lines if the trilinear coupling A_0 is kept at fixed values. Because of their

JHEP08(2005)059

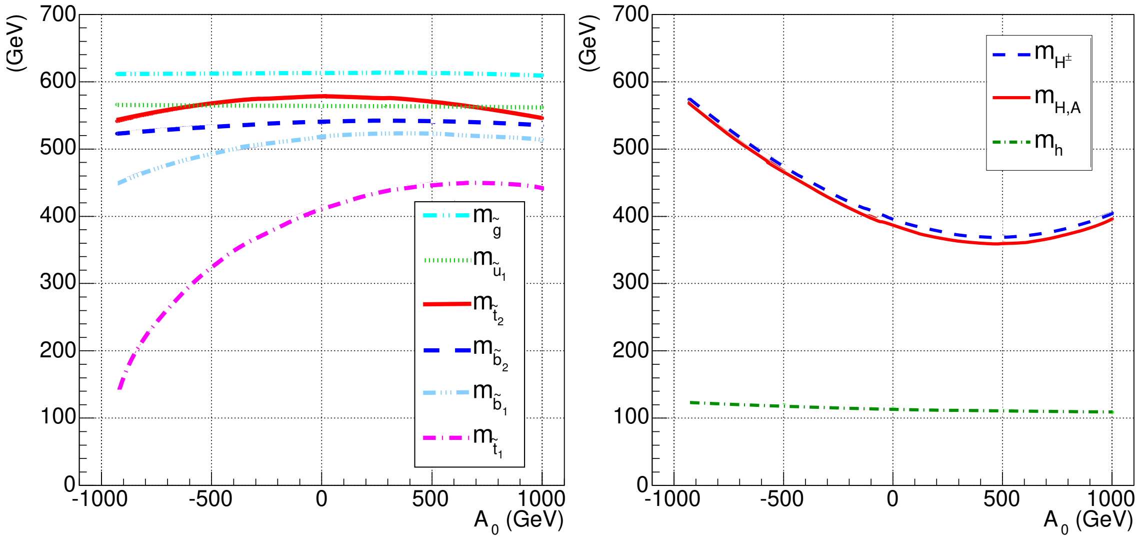

Figure 13: Gluino, squark and Higgs masses for SPS1A ($m_0 = 100$ GeV, $m_{1/2} = 250$ GeV, $\tan\beta = 10$, $\mu > 0$) as a function of A_0 obtained with ISAJET.

A_0	a	b	c $[10^{-5}]$	$m_{1/2}$ domain	m_0 domain
-2 TeV	86 ± 4	-0.04 ± 0.01	8.9 ± 0.8	$502 \div 955$ GeV	$132 \div 208$ GeV
-1.5 TeV	57 ± 2	0.081 ± 0.006	7.0 ± 0.4	$391 \div 975$ GeV	$102 \div 203$ GeV
-1 TeV	35 ± 1	0.110 ± 0.003	5.6 ± 0.2	$265 \div 985$ GeV	$71 \div 198$ GeV
-0.5 TeV	9.4 ± 0.7	0.161 ± 0.002	2.5 ± 0.2	$260 \div 985$ GeV	$51 \div 193$ GeV
0 TeV	-2 ± 1	0.184 ± 0.004	0.9 ± 0.3	$380 \div 1000$ GeV	$66 \div 193$ GeV
0.5 TeV	0 ± 2	0.177 ± 0.007	1.3 ± 0.5	$482 \div 990$ GeV	$86 \div 188$ GeV
1 TeV	15 ± 4	0.14 ± 0.01	3.5 ± 0.8	$562 \div 990$ GeV	$102 \div 188$ GeV
1.5 TeV	44 ± 8	0.08 ± 0.02	7 ± 1	$623 \div 1000$ GeV	$117 \div 193$ GeV
2 TeV	76 ± 14	0.02 ± 0.03	10 ± 2	$683 \div 1000$ GeV	$137 \div 198$ GeV
2.5 TeV	85 ± 26	0.03 ± 0.06	9 ± 4	$733 \div 990$ GeV	$158 \div 203$ GeV

Table 2: Coefficients a, b and c of the parametrisation for $\tan\beta = 5$ for different discrete values of A_0 between -2 TeV and $+2.5$ TeV. For larger or smaller A_0 values too few mSUGRA models survive the WMAP constraints to allow a reasonable parametrisation. The last two columns contain the domains for $m_{1/2}$ and m_0, respectively.

smooth narrow shape, they can be fitted by a polynomial of 2nd order:

$$m_0 = a + b \cdot m_{1/2} + c \cdot m_{1/2}^2 .$$

The coefficients of the quadratic terms are small, but they should not be neglected as $c \cdot m_{1/2}^2$ can be of the same magnitude as $b \cdot m_{1/2}$ in the allowed $m_{1/2}$ domain: the surviving mSUGRA models do not lie on a straight line but on a curve (figures 14 to 16). The parameters we obtained by using the MINUIT [29] routines are given in the tables 2 to 6 for different values of $\tan\beta$ and A_0. The numbers have been calculated from the ISAJET output.

The gaps on the fitted lines for $\tan\beta = 50$ originate from the chosen step size for m_0 (figure 4). Some plots exhibit extended areas for small m_0 and small $m_{1/2}$ (for ex-

JHEP08(2005)059

A_0	a	b	$c\ [10^{-5}]$	$m_{1/2}$ domain	m_0 domain
-2 TeV	189 ± 4	-0.02 ± 0.01	11.3 ± 0.9	$485 \div 965$ GeV	$208 \div 285$ GeV
-1.5 TeV	134 ± 2	0.034 ± 0.007	8.8 ± 0.5	$400 \div 965$ GeV	$163 \div 249$ GeV
-1 TeV	96 ± 1	0.045 ± 0.004	9.4 ± 0.3	$260 \div 954$ GeV	$117 \div 224$ GeV
-0.5 TeV	47 ± 1	0.104 ± 0.003	6.6 ± 0.3	$260 \div 939$ GeV	$76 \div 203$ GeV
0 TeV	8 ± 1	0.171 ± 0.003	2.6 ± 0.2	$260 \div 964$ GeV	$51 \div 198$ GeV
0.5 TeV	11 ± 1	0.157 ± 0.004	3.3 ± 0.3	$340 \div 980$ GeV	$66 \div 198$ GeV
1 TeV	53 ± 2	0.081 ± 0.006	7.2 ± 0.4	$390 \div 984$ GeV	$97 \div 203$ GeV
1.5 TeV	105 ± 3	0.016 ± 0.009	9.7 ± 0.6	$447 \div 980$ GeV	$132 \div 214$ GeV
2 TeV	154 ± 4	-0.02 ± 0.01	10.3 ± 0.8	$487 \div 960$ GeV	$168 \div 229$ GeV
2.5 TeV	200 ± 6	-0.05 ± 0.02	10 ± 1	$562 \div 1000$ GeV	$208 \div 259$ GeV

Table 3: Same as in table 2, but for $\tan\beta = 10$.

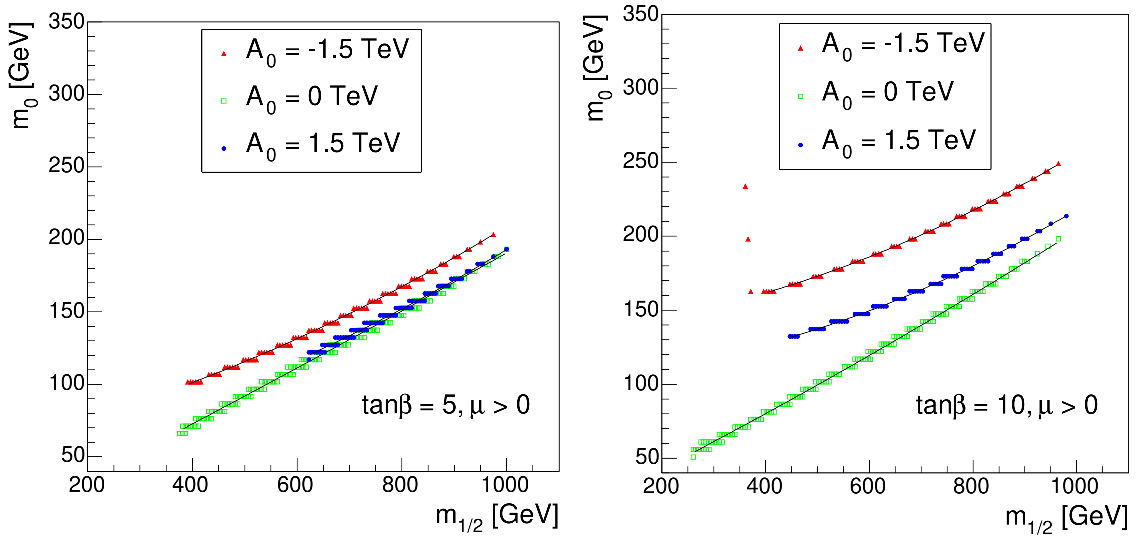

Figure 14: Allowed regions in the $m_0 - m_{1/2}$ plane, on the left for $\tan\beta = 5$ and on the right for $\tan\beta = 10$. In both plots μ is positive. The black lines are the fits given in tables 2 and 3.

A_0	a	b	$c\ [10^{-5}]$	$m_{1/2}$ domain	m_0 domain
-1.5 TeV	257 ± 2	0.071 ± 0.008	6.6 ± 0.6	$326 \div 980$ GeV	$293 \div 400$ GeV
-1 TeV	183 ± 2	0.080 ± 0.005	7.4 ± 0.4	$286 \div 965$ GeV	$212 \div 329$ GeV
-0.5 TeV	108 ± 1	0.106 ± 0.003	7.6 ± 0.3	$220 \div 975$ GeV	$136 \div 283$ GeV
0 TeV	46 ± 1	0.160 ± 0.003	5.3 ± 0.3	$245 \div 960$ GeV	$91 \div 248$ GeV
0.5 TeV	68 ± 1	0.100 ± 0.005	8.3 ± 0.4	$326 \div 970$ GeV	$111 \div 243$ GeV
1 TeV	153 ± 3	-0.005 ± 0.008	11.9 ± 0.6	$401 \div 960$ GeV	$172 \div 258$ GeV
1.5 TeV	246 ± 4	-0.07 ± 0.01	12.5 ± 0.9	$467 \div 940$ GeV	$243 \div 294$ GeV
2 TeV	327 ± 3	-0.079 ± 0.009	10.7 ± 0.7	$447 \div 985$ GeV	$314 \div 354$ GeV
2.5 TeV	410 ± 18	-0.09 ± 0.05	10 ± 4	$557 \div 819$ GeV	$390 \div 400$ GeV

Table 4: Same as in table 2, but for $\tan\beta = 20$.

A_0	a	b	c $[10^{-5}]$	$m_{1/2}$ domain	m_0 domain
-1.5 TeV	427 ± 5	0.19 ± 0.02	4 ± 1	$356 \div 799$ GeV	$499 \div 600$ GeV
-1 TeV	301 ± 2	0.190 ± 0.005	5.1 ± 0.4	$281 \div 995$ GeV	$358 \div 540$ GeV
-0.5 TeV	176 ± 1	0.219 ± 0.004	5.4 ± 0.3	$245 \div 1000$ GeV	$231 \div 448$ GeV
0 TeV	88 ± 1	0.251 ± 0.003	4.7 ± 0.2	$245 \div 1000$ GeV	$151 \div 388$ GeV
0.5 TeV	138 ± 1	0.139 ± 0.004	9.7 ± 0.3	$311 \div 1000$ GeV	$191 \div 373$ GeV
1 TeV	282 ± 2	0.001 ± 0.007	13.1 ± 0.5	$376 \div 995$ GeV	$302 \div 413$ GeV
1.5 TeV	432 ± 3	-0.058 ± 0.009	12.2 ± 0.6	$391 \div 985$ GeV	$428 \div 494$ GeV
2 TeV	577 ± 5	-0.08 $\pm$ 0.01	10.3 ± 1.0	$517 \div 980$ GeV	$565 \div 600$ GeV

Table 5: Same as in table 2, but for $\tan\beta = 35$.

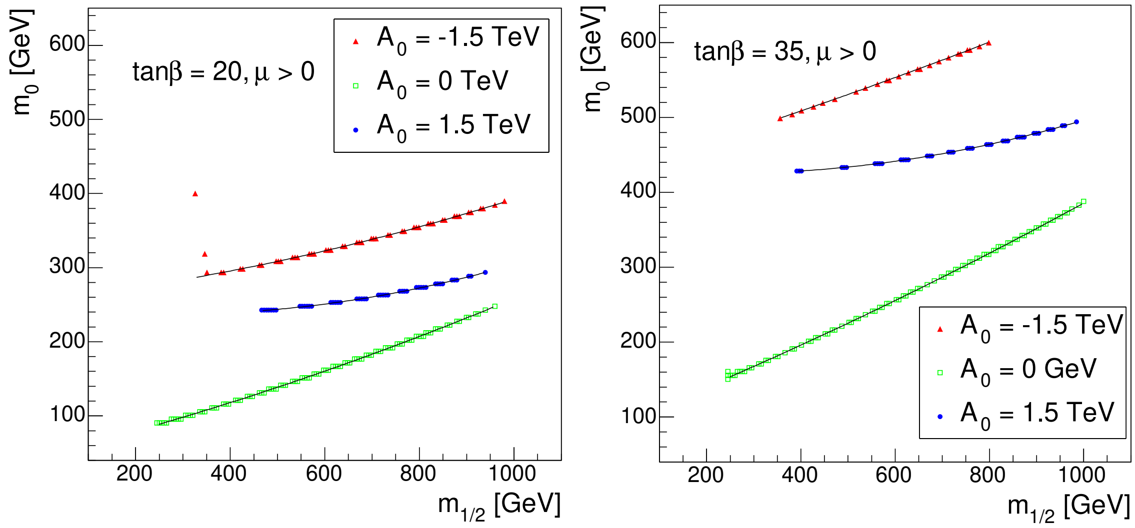

Figure 15: Allowed regions in the $m_0 - m_{1/2}$ plane for $\tan\beta = 20$ (left) and for $\tan\beta = 35$ (right). In both plots μ is positive. The black lines are the fits given in tables 4 and 5.

ample figure 16 for $A_0 = 0\,\text{TeV}$). These regions are excluded in the fits, since a proper parametrisation would be much more involved.

The relic density develops a strong dependence on the common gaugino mass $m_{1/2}$ for small values near the lower bound coming from the accelerator constraints. Consequently, unexpectedly large m_0 values (for small $m_{1/2}$) can lead to $\Omega_\chi h^2$ values within the WMAP range. This behaviour manifests itself e.g. in the isolated points in figure 14 ($\tan\beta = 10$) and in figure 15 ($\tan\beta = 20$), for $A_0 = -1500\,\text{GeV}$.

The separation between the lines for different A_0 becomes larger with increasing $\tan\beta$ and increasing $|A_0|$ (figures 14 to 16). For $\tan\beta = 5$ the corresponding splitting in m_0 is smaller than 90 GeV, while for $\tan\beta = 50$ it can reach about 700 GeV. For negative A_0 the shift in m_0 is larger than for positive values, but always to higher m_0 values so that the minimal m_0 values are obtained for vanishing A_0. For small $\tan\beta$ the dominant contribution to the annihilation cross section may come from the t-channel stau exchange (especially in the coannihilation region $m_0 \ll m_{1/2}$). The running of the stau masses depends quadratically on A_0. For large values of $\tan\beta$ the rapid annihilation via a s-channel

A_0	a	b	c $[10^{-5}]$	$m_{1/2}$ domain	m_0 domain
-2 TeV	830 ± 6	0.30 ± 0.02	4 ± 1	$311 \div 1085$ GeV	$922 \div 1200$ GeV
-1.5 TeV	635 ± 3	0.294 ± 0.006	6.1 ± 0.3	$421 \div 1416$ GeV	$770 \div 1175$ GeV
-1 TeV	425 ± 5	0.35 ± 0.01	5.5 ± 0.5	$472 \div 1427$ GeV	$605 \div 1035$ GeV
-0.5 TeV	249 ± 1	0.395 ± 0.003	5.4 ± 0.2	$290 \div 1427$ GeV	$352 \div 922$ GeV
0 TeV	152 ± 1	0.401 ± 0.004	6.3 ± 0.2	$390 \div 1397$ GeV	$314 \div 833$ GeV
0.5 TeV	236 ± 2	0.250 ± 0.005	12.2 ± 0.3	$430 \div 1286$ GeV	$365 \div 757$ GeV
1 TeV	429 ± 1	0.100 ± 0.004	15.3 ± 0.2	$341 \div 1286$ GeV	$478 \div 808$ GeV
1.5 TeV	630 ± 5	0.05 ± 0.01	13.2 ± 0.5	$532 \div 1306$ GeV	$694 \div 922$ GeV
2 TeV	852 ± 4	0.000 ± 0.009	12.2 ± 0.5	$411 \div 1306$ GeV	$871 \div 1061$ GeV
2.5 TeV	1073 ± 39	-0.03 $\pm$ 0.08	11 ± 4	$653 \div 1155$ GeV	$1099 \div 1187$ GeV

Table 6: Same as in table 2, but for $\tan\beta = 50$.

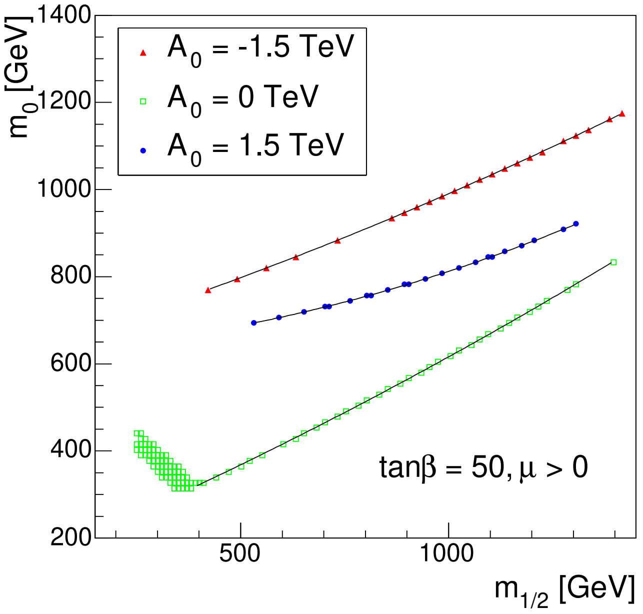

Figure 16: Allowed regions in the $m_0 - m_{1/2}$ plane for $\tan\beta = 50$ and $\mu > 0$. The black lines are the fits given in table 6.

Higgs boson exchange can be dominant. The Higgs masses depend linearly as well as a quadratically on A_0 [1]. These dependencies of the sparticles and Higgs bosons masses on A_0 (figure 13) affect the cross sections and therefore also the relic density [30]. They explain the different behaviour for positive and negative values of A_0.

7. Conclusions

By including the trilinear scalar coupling A_0 as a free parameter in the range of ± 4 TeV large regions in the $m_0 - m_{1/2}$ plane of mSUGRA models turn out to be consistent with the WMAP data. Fixing this coupling results in narrow lines strongly depending on A_0. Large m_0 values (e.g. up to 2 TeV for $\tan\beta = 50$) are allowed for $|A_0| \gg 0$. Using the

JHEP08(2005)059

mSUGRA models generated with the ISAJET program we constructed a parametrisation for the common scalar mass m_0 as function of the common gaugino mass $m_{1/2}$ for several fixed values of A_0 and tanβ. The same qualitative behaviour is found using the SuSpect code. We analysed the discrepancies between the two Monte Carlo programs and traced them back to slightly different mass spectra and couplings, which result in different values of $\Omega_\chi h^2$. As the WMAP cut on the relic density is very tight a small difference may have a big impact on the mSUGRA parameter space.

In addition we started to study the effect of A_0 on the masses of the sparticles. The gluinos and the first two generations of the squarks are insensitive to A_0, hence most of the allowed mSUGRA models still lie within the reach of the LHC. However, the third generation of squarks and the heavier Higgs bosons depend significantly on A_0.

Acknowledgments

We would like to thank Michael Spira for helpful theoretical discussions, Luc Pape for useful comments and both for careful reading of this paper. We also thank Josep Flix for providing us with helpful code concerning the linking between the MC programs.

References

[1] See e.g. V. Bertin, E. Nezri and J. Orloff, *Neutrino indirect detection of neutralino dark matter in the CMSSM*, *Eur. Phys. J.* **C 26** (2002) 111 [hep-ph/0204135];
J.R. Ellis, S. Heinemeyer, K.A. Olive and G. Weiglein, *Indirect sensitivities to the scale of supersymmetry*, *JHEP* **02** (2005) 013 [hep-ph/0411216].

[2] WMAP collaboration, C.L. Bennett et al., *First year Wilkinson Microwave Anisotropy Probe (WMAP) observations: preliminary maps and basic results*, *Astrophys. J. Suppl.* **148** (2003) 1 [astro-ph/0302207];
WMAP collaboration, D.N. Spergel et al., *First year Wilkinson Microwave Anisotropy Probe (WMAP) observations: determination of cosmological parameters*, *Astrophys. J. Suppl.* **148** (2003) 175 [astro-ph/0302209].

[3] J.R. Ellis, K.A. Olive, Y. Santoso and V.C. Spanos, *Supersymmetric dark matter in light of WMAP*, *Phys. Lett.* **B 565** (2003) 176 [hep-ph/0303043];
M. Battaglia, A. De Roeck, J.R. Ellis, F. Giannotti, K.A. Olive and L. Pape, *Updated post-WMAP benchmarks for supersymmetry*, *Eur. Phys. J.* **C 33** (2004) 273 [hep-ph/0306219].

[4] E. Witten, *Mass hierarchies in supersymmetric theories*, *Phys. Lett.* **B 105** (1981) 267.

[5] J. Wess and B. Zumino, *Supergauge transformations in four-dimensions*, *Nucl. Phys.* **B 70** (1974) 39;
P. Fayet and S. Ferrara, *Supersymmetry*, *Phys. Rept.* **32** (1977) 249;
H.P. Nilles, *Supersymmetry, supergravity and particle physics*, *Phys. Rept.* **110** (1984) 1;
R. Barbieri, *Looking beyond the Standard Model: the supersymmetric option*, *Riv. Nuovo Cimento* **11N4** (1988) 1.

[6] H.E. Haber and G.L. Kane, *The search for supersymmetry: probing physics beyond the standard model*, *Phys. Rept.* **117** (1985) 75.

[7] P. Fayet, *Spontaneously broken supersymmetric theories of weak, electromagnetic and strong interactions*, *Phys. Lett.* **B 69** (1977) 489;
S. Dimopoulos and H. Georgi, *Softly broken supersymmetry and* SU(5), *Nucl. Phys.* **B 193** (1981) 150;
N. Sakai, *Naturalness in supersymmetric 'GUTs'*, *Z. Physik* **C 11** (1981) 153;
U. Amaldi, W. de Boer and H. Furstenau, *Comparison of grand unified theories with electroweak and strong coupling constants measured at LEP*, *Phys. Lett.* **B 260** (1991) 447.

[8] L.E. Ibáñez and G.G. Ross, $\mathrm{SU}(2)_L \times \mathrm{U}(1)$ *symmetry breaking as a radiative effect of supersymmetry breaking in GUTs*, *Phys. Lett.* **B 110** (1982) 215.

[9] CDF collaboration, D0 collaboration, Tevatron Electroweak Working Group, *Combination of CDF and D0 results on the top-quark mass*, `hep-ex/0507091`.

[10] H. Goldberg, *Constraint on the photino mass from cosmology*, *Phys. Rev. Lett.* **50** (1983) 1419;
J.R. Ellis, J.S. Hagelin, D.V. Nanopoulos, K.A. Olive and M. Srednicki, *Supersymmetric relics from the big bang*, *Nucl. Phys.* **B 238** (1984) 453;
M. Drees and M.M. Nojiri, *The neutralino relic density in minimal $N = 1$ supergravity*, *Phys. Rev.* **D 47** (1993) 376 [`hep-ph/9207234`].

[11] G.R. Farrar and P. Fayet, *Phenomenology of the production, decay and detection of new hadronic states associated with supersymmetry*, *Phys. Lett.* **B 76** (1978) 575;
F. Zwirner, *Observable $\Delta B = 2$ transitions without nucleon decay in a minimal supersymmetric extension of the Standard Model*, *Phys. Lett.* **B 132** (1983) 103;
L.J. Hall and M. Suzuki, *Explicit R parity breaking in supersymmetric models*, *Nucl. Phys.* **B 231** (1984) 419;
J.R. Ellis, G. Gelmini, C. Jarlskog, G.G. Ross and J.W.F. Valle, *Phenomenology of supersymmetry with broken R parity*, *Phys. Lett.* **B 150** (1985) 142;
G.G. Ross and J.W.F. Valle, *Supersymmetric models without R parity*, *Phys. Lett.* **B 151** (1985) 375;
S. Dawson, *R parity breaking in supersymmetric theories*, *Nucl. Phys.* **B 261** (1985) 297.

[12] A.H. Chamseddine, R. Arnowitt and P. Nath, *Locally supersymmetric grand unification*, *Phys. Rev. Lett.* **49** (1982) 970;
K. Inoue, A. Kakuto, H. Komatsu and S. Takeshita, *Low-energy parameters and particle masses in a supersymmetric grand unified model*, *Prog. Theor. Phys.* **67** (1982) 1889; *Aspects of grand unified models with softly broken supersymmetry*, *Prog. Theor. Phys.* **68** (1982) 927, erratum *ibid.* **70** (1983) 330; *Renormalization of supersymmetry breaking parameters revisited*, *Prog. Theor. Phys.* **71** (1984) 413;
L. Alvarez-Gaumé, M. Claudson and M.B. Wise, *Low-energy supersymmetry*, *Nucl. Phys.* **B 207** (1982) 96;
J.R. Ellis, D.V. Nanopoulos and K. Tamvakis, *Grand unification in simple supergravity*, *Phys. Lett.* **B 121** (1983) 123.

[13] W. de Boer, *Search for SUSY and Higgs particles*, `hep-ph/9808448`.

[14] B.C. Allanach et al., *The SNOWMASS points and slopes: benchmarks for SUSY searches*, *Eur. Phys. J.* **C 25** (2002) 113 [`hep-ph/0202233`].

[15] G.A. Blair, W. Porod and P.M. Zerwas, *The reconstruction of supersymmetric theories at high energy scales*, *Eur. Phys. J.* **C 27** (2003) 263 [`hep-ph/0210058`].

[16] G. Jungman, M. Kamionkowski and K. Griest, *Supersymmetric dark matter*, *Phys. Rept.* **267** (1996) 195 [hep-ph/9506380].

[17] P. Binetruy, G. Girardi and P. Salati, *Constraints on a system of two neutral fermions from cosmology*, *Nucl. Phys.* **B 237** (1984) 285;
K. Griest and D. Seckel, *Three exceptions in the calculation of relic abundances*, *Phys. Rev.* **D 43** (1991) 3191.

[18] A. Djouadi, J.-L. Kneur and G. Moultaka, *Suspect: a Fortran code for the supersymmetric and Higgs particle spectrum in the MSSM*, hep-ph/0211331, http://www.lpta.univ-montp2.fr/users/kneur/Suspect/.

[19] F.E. Paige, S.D. Protopescu, H. Baer and X. Tata, *Isajet 7.69: a Monte Carlo event generator for pp, $\bar{p}p$ and e^+e^- reactions*, hep-ph/0312045, http://www.phy.bnl.gov/~isajet/.

[20] J. Flix, private communication.

[21] P. Gondolo, J. Edsjö, L. Bergström, P. Ullio and E.A. Baltz, *Darksusy: a numerical package for dark matter calculations in the MSSM*, astro-ph/0012234, http://www.physto.se/~edsjo/darksusy/.

[22] N. Ghodbane and H.-U. Martyn, *Compilation of SUSY particle spectra from Snowmass 2001 benchmark models*, hep-ph/0201233;
B.C. Allanach, S. Kraml and W. Porod, *Theoretical uncertainties in sparticle mass predictions from computational tools*, *JHEP* **03** (2003) 016 [hep-ph/0302102];
G. Belanger, S. Kraml and A. Pukhov, *Comparison of SUSY spectrum calculations and impact on the relic density constraints from WMAP*, *Phys. Rev.* **D 72** (2005) 015003 [hep-ph/0502079].

[23] Muon g-2 collaboration, G.W. Bennett et al., *Measurement of the negative muon anomalous magnetic moment to 0.7 ppm*, *Phys. Rev. Lett.* **92** (2004) 161802 [hep-ex/0401008].

[24] Particle Data Group collaboration, K. Hagiwara et al., *Review of particle physics*, *Phys. Rev.* **D 66** (2002) 010001, http://pdg.lbl.gov/pdg.html.

[25] P. Gondolo, J. Edsjö, P. Ullio, L. Bergström, M. Schelke and E.A. Baltz, *Darksusy: computing supersymmetric dark matter properties numerically*, *JCAP* **07** (2004) 008 [astro-ph/0406204].

[26] L. Alvarez-Gaumé, J. Polchinski and M.B. Wise, *Minimal low-energy supergravity*, *Nucl. Phys.* **B 221** (1983) 495;
J.M. Frere, D.R.T. Jones and S. Raby, *Fermion masses and induction of the weak scale by supergravity*, *Nucl. Phys.* **B 222** (1983) 11;
M. Claudson, L.J. Hall and I. Hinchliffe, *Low-energy supergravity: false vacua and vacuous predictions*, *Nucl. Phys.* **B 228** (1983) 501;
C. Kounnas, A.B. Lahanas, D.V. Nanopoulos and M. Quiros, *Low-energy behavior of realistic locally supersymmetric grand unified theories*, *Nucl. Phys.* **B 236** (1984) 438;
J.P. Derendinger and C.A. Savoy, *Quantum effects and* $\mathrm{SU}(2) \times \mathrm{U}(1)$ *breaking in supergravity gauge theories*, *Nucl. Phys.* **B 237** (1984) 307.

[27] A. Riotto and E. Roulet, *Vacuum decay along supersymmetric flat directions*, *Phys. Lett.* **B 377** (1996) 60 [hep-ph/9512401].

[28] http://cmsinfo.cern.ch/Welcome.html.

[29] F. James and M. Roos, *'Minuit' a system for function minimization and analysis of the parameter errors and correlations*, *Comput. Phys. Commun.* **10** (1975) 343; `http://wwwasdoc.web.cern.ch/wwwasdoc/WWW/minuit/minmain/minmain.html`.

[30] L.S. Stark et al., in preparation.